Automotive Experiences
Vol. 6 No. 2 (2023) pp. 336-358
p-ISSN: 2615-6202 e-ISSN: 2615-6636

Research Paper

Mechanical Characteristics of Distributed Electric Wheel Loader in Shoveling Condition

Xiaotao Fei[1,2], **Han Senrui**[3], **Shaw Voon Wong**[1], **Muhammad Amin Azman**[1], **Han Yunwu**[2]

[1]Department of Mechanical & Manufacturing, Faculty of Engineering, Universiti Putra Malaysia, 43400, Malaysia
[2]Jiangsu Vocational College of Electronics and Information, 223003, China
[3]College of Ecology and Environment, Hainan Tropical Ocean University, 572022, China

wongsv@upm.edu.my

https://doi.org/10.31603/ae.9024

Check for updates

Published by Automotive Laboratory of Universitas Muhammadiyah Magelang collaboration with Association of Indonesian Vocational Educators (AIVE)

Article Info
Submitted:
20/04/2023
Revised:
13/08/2023
Accepted:
15/08/2023
Online first:
27/08/2023

Abstract

Multi-bridge centralized drive wheel loaders can produce parasitic power to waste energy and aggravate tire wear. Distributed Electric Wheel Loader(DEWL) is a new structure with two drive motors that can be controlled independently or in concert. Hence, this study investigates the mechanical characteristics of DEWL in its shoveling condition. Firstly, for the DEWL, dynamic models are established including running and shoveling conditions, on the basis of automobile theory. Secondly, a simplified structural model of DEWL is used to construct the mechanical equations, and the theoretical derivation is utilized to analyze the forces on wheels during different driving modes of running and shoveling conditions. Finally, the free shoveling of dry sands and gravel materials is tested by a ZL50GV-EV DEWL, and the drive forces of three drive modes on horizontal concrete pavement are tested. The results show that the parasitic power is generated when the driving motor has a larger speed than that of the other motor, which is caused by the movement of the loader's center of gravity. The driving torques generated by the motors are basically the same when the DEWL is in front-drive mode and rear-drive mode at the setting speed of 600rpm, whether it is running forward or backward, with a torque fluctuation of 0.16%-1.28% and a power fluctuation of 0.02%-1.29%. The DEWL consumes more power in dual-drive mode than in single drive if it is controlled in speed-target mode.

Keywords: Electric wheel loader; Parasitic power; Shoveling condition; Force analysis; Mechanical characteristics

1. Introduction

Loaders, also called wheel loaders (WL) or shoveling loaders, which constitute one of the most important off-road vehicles since they can exhibit high performance and flexibility for transporting materials in ports, mines and construction sites [1]. With enormous amount of WLs are working in the world, it makes sense to diminish energy consumption of WLs. Literature are mainly studied on the energy-saving control methods that are widely applied to WLs include load-sensitive hydraulic system [2]–[4], hydrostatic drive technology [5], [6], engine energy-saving technology [7], [8], and hybrid power technology [9]–[11]. As the research and utilization of electrification becomes a trend in area of vehicles [12], the research of electric wheel loaders (EWL) has been paid more attention on. Jin [13] applied the Permanent Magnet Synchronous Motor (PMSM) to a conventional WL, conducted that the efficiency of PMSM reaches 95% at the vehicle velocity of 5 km/h, by test of running, dragging and steering conditions. But they haven't tested on shoveling condition which is the largest energy consuming condition. Yang [14] mainly conducted performance comparison tests for EWL and traditional loaders, including operational performance and noise performance tests. The test results indicated that operational performance and noise performance

Nomenclature	
DEWL	= Distributed Electric Wheel Loader
EWL	= Electric Wheel Loader
PMSM	= Permanent Magnet Synchronous Motor
SMR	= Switched Reluctance Motor
WL	= Wheel Loader

are both better than that of conventional ones. Li, X, et al. [15] investigated the operational performance of EWL matched with three types of motors, carried out that different types of motors should be applied in drive system and hydraulic system to get best performance. Cao, B. W, et al. [16] proposed the method of adjusting the attitude of working device to realize the anti-skid shovel control of WL. **Table 1** shows the more detailed research on energy-saving of WL or EWLs.

Distributed electric wheel loader (DEWL) takes two motors respectively installed in front and rear part. However, there is few literature [17], [18] discussing about how to distribute the drive torques of front and rear motors which will result in that the motors work at high efficiency speed range so as to obtain energy saving, when DEWL is working. WL is a kind of multi-axles drive vehicle, in order to achieve a better overall drive adhesion effect, most diesel engine drive WLs [19] are equipped with a transfer case to transmit power to the front drive axle and the rear drive axle, due to their structural characteristics. This results in the rotation speeds of the front and rear wheels being approximately the same when the WL is working. Due to the change in the bucket position and the center of gravity of the excavated material when the WL is working, the vertical pressure of the front and rear wheels on the ground will change, which can have two consequences. The first is that, for wheels with decreasing vertical pressure, the ground may not provide enough adhesion, causing the tire to slip and generate parasitic power [20], including necessary parasitic power and unnecessary parasitic power [21]. Yang [21] proves that parasitic power can account for up to 45% of the total power of the centralized EWL in some cases. The second is that, for wheels with an increasing vertical load, the rolling resistance torque may be greater than the rated torque of the motor on that transaxle, causing the motor to heat up and over-load.

EWLs are driven by electric motors, which produce driving force to transmission system and also generate electricity when the velocity decreases [22]. The motor has the mechanical characteristics of high torque at low speed, which is suitable for WLs in shoveling and carrying material conditions [23]. A WL usually runs at low speed [24] in various fixed places which is quite different from a road vehicle running at high speed in continuously changing road, but the theory of classical vehicle dynamics can be applied to analyze the driving process of a WL.

The load of the tires changes most frequently, and the radius of the tires also changes accordingly, during the shoveling process of the WL. In order to seek the most reasonable way to coordinate and control the motor-driven loader, this paper calculates and analyzes the torque, and the resistance to the wheels. And with the parameters of a certain pure electric loader, the rationality of the calculation is verified by the test results. The contribution of the paper is: it proves that the rolling resistance on an EWL is the same regardless of its driven by the front wheel or the rear wheel, and is not affected by the tire radius, by means of the derivation of the formula. The conclusions obtained in this study provide theoretical support and practical proof for the design and power distribution control of the new DEWL.

The article consists of seven parts. Section 2 develops the dynamic models of DEWL, the running model and the shoveling model are built and analyzed respectively. Section 3 analyses three different drive forms of EWL in the case of rear wheel drive, front wheel drive and dual-motor drive, derives the expressions of rolling resistance on the front and rear wheels under different driving conditions, points out the characteristics of DEWL in shoveling condition. Section 4 carries out a series of experiments and tests on EWL free shoveling condition and driving forces of running condition. Section 5 validates the correctness of theoretical derivation through the analyzing the test results. Section 6 discusses the application value of the mechanical characteristics of DEWL in shoveling condition. Section 7 provides a summary of the study.

2. Dynamic Model of DEWL

2.1. Running Model

The dynamic running model of the WL's running mechanism is similar to that of a two-axle

Table 1. A simple review of energy-saving research on electric wheel loaders

Ref.	Title	Main Content	Research Method	Main Related Results	Limitations
[25]	Shoveling behavior and resistance of loader bucket	Through a study in the process of shovel cut-in and ore-shoveling, their behavior and resistance are discussed in detail.	1. Theoretical analysis 2. Formula derivation	The calculation method of bucket insertion resistance based on the multi-coefficient method is thoroughly investigated, and a suitable insertion resistance calculation method for small particle diameters is proposed.	1. The experimental validation has not been applied. 2. The specific loading conditions was not taken into consideration.
[26]	Design and research on wheel-driven systems of electric loaders	The PMSM was introduced to the wheel-driven system of EWL	1. Bench testing 2. Heavy-loading condition testing	1. Driving efficiency of electric wheel is greater than 95% at the speed of 5 km/h; 2. Driving efficiency of electric wheel is greater than 92% at the maximum traction force of 2.67 kN.	The running, dragging, and steering conditions were tested but they did not test the shoveling condition
[14]	Comparative Test Research on Performance of Electric Loader and Traditional Loader	The operation performance and noise performance were compared between EWL and a conventional WL by testing.	1. Cycle condition test 2. Driving experience	1. The average cycling time of EWL is 266 s which is shorter than that of conventional ones with 300 s; 2. Noise test results outside the WL show that the EWL is 9dB(A) lower than the traditional WL.	1. Some evaluation indicators are not the same, such as the operation efficiency and energy consumption. 2. The test results are deeply affected by the drivers' skill.
[27]	Integrated wheel loader simulation model for improving performance and energy flow	1. A driver model for a WL's V-cycle working pattern was developed. 2. A 3D dynamic simulation model was developed to analyze the working performance of the WL.	1. Modeling 2. Simulation research	1. A driver model of WL for V-pattern working based on experimental test data was developed and validated by comparing with based on experimental test data. 2. The working performance and analyze energy flow of V-pattern working were evaluated	The powertrain and dynamic models developed for conventional WL are more complicated compared with EWL.
[28]	Energy management of hybrid electric vehicles with battery aging considerations: Wheel loader case study	1. A differential battery capacity fade model is used for energy management analysis. 2. A two-step algorithm is proposed to identify the aging model parameters. 3. The controller is then implemented for a hybrid electric wheel loader to demonstrate its effectiveness.	1. Modeling 2. Simulation research 3. Case study	Short and long term simulations were performed on four WL cycles to test the energy management strategy of the hybrid EWL. For the hybrid EWL studied, battery life was extended but fuel consumption increased.	1. The models of hybrid electric powertrains were complex; 2. They haven't tested in real working or shoveling conditions of
[15]	Operating performance of pure electric loaders with different types of motors based on simulation analysis	1. Three types of motors were applied to drive the same EWL by joint simulation; 2. The characteristics of the walking system with three motors, including the shoveling and unloading performance of the hydraulic system with three motors, were analyzed.	1. Modeling 2. Simulation research 3. Experiment on real working conditions.	1. The SRM-driven walking system provides the loader with greater material insertion capability than either of the other two types of motors, in terms of speed and depth of insertion. 2. When using SRM, the loader's walking system has a higher gradient and the acceleration is not inferior to the other two types of motors.	Variable-speed control strategies, new electric drive hydraulic control strategies and dynamic arm energy recovery are still the key technologies that will limit the development of EWLs [29].

vehicle when the loader bucket is not in contact with the ground and the stockpile, if the steering of the loader is not taken into consideration. The driving function [30] is shown in Eq. (1).

Generally, the speed of a WL is lower than 30km/h when it is working. According to the principle of automobile dynamics, the air resistance it receives can be expressed by Eq. (2).

$$F_t = F_f + F_w + F_i + F_i \tag{1}$$

where, F_t is the drive force for the vehicle,F_f is the rolling resistance between the ground and the tire, F_w is the air resistance suffered by the vehicle, F_i is the slope resistance encountered by the vehicle when climbing a slope, and F_j is the acceleration resistance generated during the acceleration process of the vehicle.

$$F_w = \frac{C_D \cdot A \cdot u_a^2}{21.15} \tag{2}$$

where, C_D is the coefficient of air resistance, A represents the windward area of the vehicle, u_a is the running speed of WL. Compared with the rolling resistance, the air resistance of the WL at low speed is negligible.

Although the working ground of WLs is uneven, it can still be simplified as a horizontal road in the study in order to facilitate the analysis, so that the slope resistance is viewed zero. The rolling resistance of the WL on the ground against it is shown in Eq. (3).

$$F_f = G \cdot f \tag{3}$$

where,f is the coefficient of rolling resistance, it can be obtained by experiment [31]. **Table 2** shows the rolling resistance coefficient values of the WL on different road surfaces.

The forces acted on an EWL in shoveling condition are also affected by the state of the bucket [32]. When the bucket is held in the air by the lifting arm, the full weight of the WL acts on the front and rear wheels is the same as an ordinary two-axles vehicle regardless of the gravity of the material in the bucket. In this case, the forces an EWL receives include the gravity G of the EWL itself, the ground rolling resistance F_{Wl_ff} and the vertical upward support force F_{Wl_zf} received by the front wheel, the ground rolling resistance F_{Wl_fr} and the ground vertically upward support force F_{Wl_zr} received by the rear wheel, and the driving torque T_{Wl_f} & T_{Wl_r} acting on the front driving wheel and the rear driving wheel respectively, which are shown in **Figure 1**.

2.2. *Shoveling Model*

When the bucket is put down by the lifting arm to contact with the ground for shoveling materials, all and part of the forces on the EWL will change. In this case, the bucket is subjected to the resistance F_{Bct} from the material and the ground, which is marked with red. This force can be decomposed into two components, namely the resistance F_{Bct_x} in the horizontal direction opposite to the speed of the EWL and F_{Bct_y} in the vertical direction, as shown in **Figure 2**.

When this occurs, the vertical force on the front and rear wheels of the WL will also change. Besides, the horizontal force of the front and rear wheels will also be affected and changed. This is because the WL should always be in a state of force balance in the plane. Assuming that the EWL has only one front motor drive, the driving force F_t can be expressed by Eq. (4).

Table 2. The value of rolling resistance on various road surfaces

Type of road surface	Coefficient of rolling resistance
Good asphalt or concrete pavement	0.010-0.108
General asphalt or concrete pavement	0.018-0.020
macadam pavement	0.020-0.025
Good pebble pavement	0.025-0.030
Chuckhole pebble pavement	0.035-0.050
Dry compact earthen road	0.025-0.035
Wet compact earthen road	0.050-0.150
Muddy soil road	0.100-0.250
Dry sand pavement	0.100-0.300
Wet sand pavement	0.060-0.150
Frozen pavement	0.015-0.030
Compact snow surface	0.030-0.050

$$F_t = \frac{T_{mot} \cdot i \cdot \eta_T}{R} \tag{4}$$

When the bucket is applied to shovel material in the working process of the EWL. As a whole, the external forces, including the gravity of the bucket and the material, on the bucket of the EWL can be equivalent to the forces acting on the tip of the bucket. This force can be decomposed into horizontal force F_{Bct_x} and vertical force F_{Bct_y}. In this case, the main external forces acting on the EWL are shown in **Figure 3**. Where, point M locates at the mass center of the EWL, l_{Br} represents the distance from the tip of bucket to the front axle in horizontal direction, a represents the distance from the front axle to the center of mass in horizontal direction, b represents the distance from the center of mass to the rear axle in horizontal direction. Besides, the sum of a and b is the wheelbase of the EWL, marked with l in this paper.

According to the principle of force balance, EWL should achieve the balance of the following groups of forces, which are shown in Eq. (5).

$$\begin{cases} \sum F_{x_i} = 0 \\ \sum F_{y_i} = 0 \\ \sum T_{z_i} = 0 \end{cases} \tag{5}$$

where, F_{x_i} indicates all the forces on EWL in horizontal direction, F_{y_i} represents all the forces on EWL in vertical direction, and T_{z_i} refers to all the torques acting on EWL in the direction perpendicular to the plane of the figure.

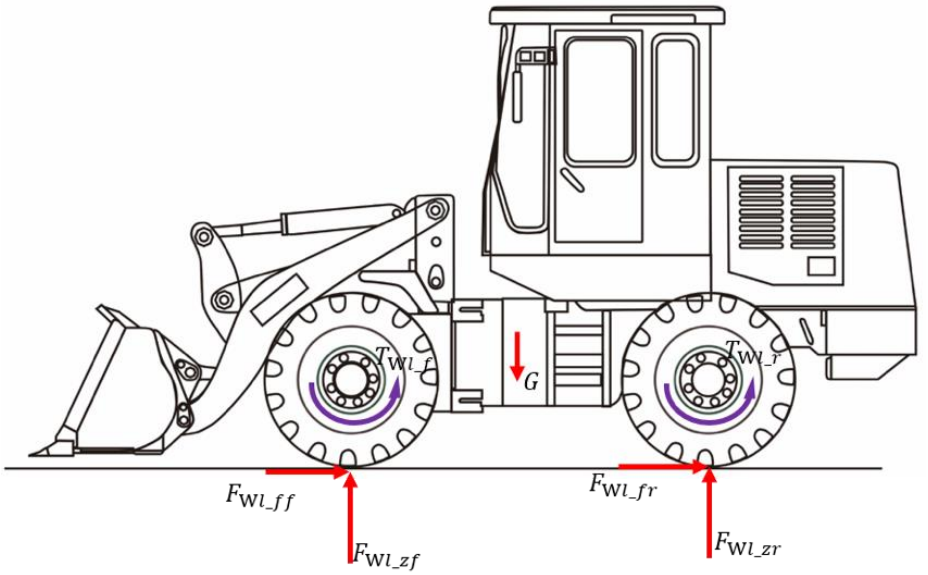

Figure 1. The forces on an EWL for constant running condition

Figure 2. A force generated when the bucket touches against ground in shoveling condition

3. Analysis of Driving Theory

Based on vehicle dynamics [33], the walking mechanism of EWL is assumed and simplified, and the driving theory analysis can be carried out under different wheel radius conditions. Similar to a two-wheel bicycle model [34], the structure of the EWL can be simplified as a front wheel and a rear wheel rigidly connected together. The interaction force between the two wheels is transmitted through a stiff connector when driving, as shown in **Figure 4**.

3.1. Force Analysis on Rear-wheel Drive

On a simplified structure of an EWL in **Figure 4**, r_1 is the radius of front wheel, r_2 is the radius of rear wheel. The forces on the rear wheel are as follows when the EWL is driven independently by rear wheel. The positive pressure of the rear wheel on the ground caused by the gravity is marked with N_2. The reverse force that the rear wheel subjected to when driving is marked with F_{Wl_tr}. The rolling resistance of rear wheel is F_{Wl_fr}, and the vertical support force that the ground to the rear wheel is F_{Wl_zr}.The forces on the front wheel are as follows. The positive pressure of the front wheel on the ground caused by the gravity is marked with N_1. The rolling resistance of front wheel is F_{Wl_ff}, and the vertical support force that the ground to the front wheel is F_{Wl_zf}.

For the convenience of analysis, the structure in **Figure 4** can be divided into two systems, including the front-wheel system shown in **Figure 5** and the rear-wheel system shown in **Figure 6**, which can be analyzed independently. Because it is rear-wheel drive, the front-wheel system of EWL will receive a thrust F_1 from the rear-wheel system, and the rear-wheel system will receive a reaction force F_1' from the front-wheel system. These two forces are equal in magnitude and opposite in direction.

3.2. Force Analysis on Front-wheel Drive

When the research object EWL is driven by front wheel, the forces on the simplified structure is shown in **Figure 7**. Compared with the previous situation, the forces on the rear wheel lacks the driving force F_{Wl_tr} and a driving force F_{Wl_tf} on the front wheel is added, while the others remain unchanged.

The structure can also be divided into two systems for analysis in the case of front-wheel drive, including the rear-wheel system shown in **Figure 8** and the front-wheel system shown in **Figure 9**. The front-wheel system generates a drag force, marked with F_2, on the rear-wheel system, and a reverse force F_2' from the rear-wheel system will act on the front-wheel system consequently. F_2 and F_2' are equal in magnitude and opposite in direction.

3.3. Theoretical Analysis on Individual Drive

Firstly, the force analysis of EWL is carried out under the condition of rear-wheel individually drive. In the front-wheel system, the contact point between the tire and the ground is O_1, which can be selected for force equilibrium analysis. According to Eq. (3) and Eq. (5), the force equilibrium of point O_1 in horizontal and vertical directions can be expressed by Eq. (6).

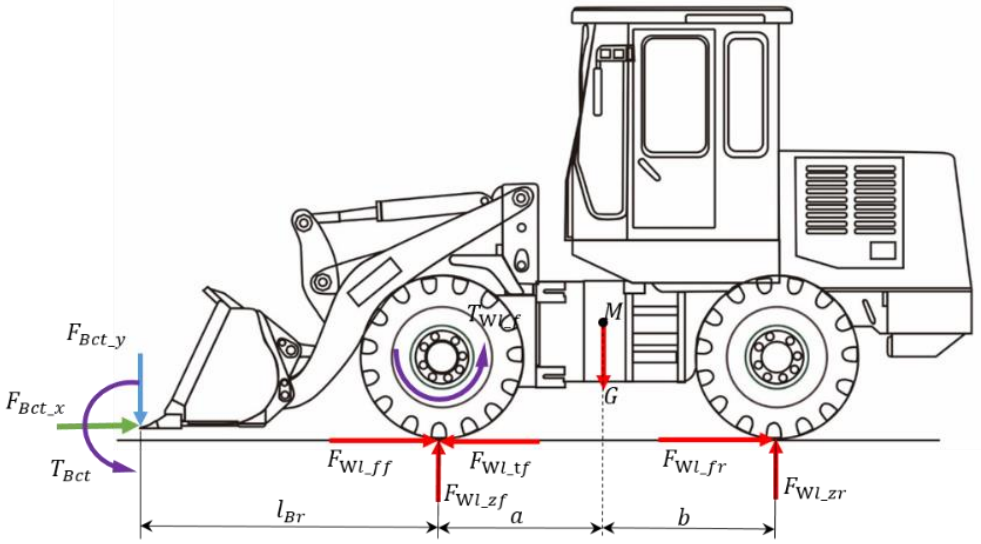

Figure 3. The forces on an EWL of a simplified case

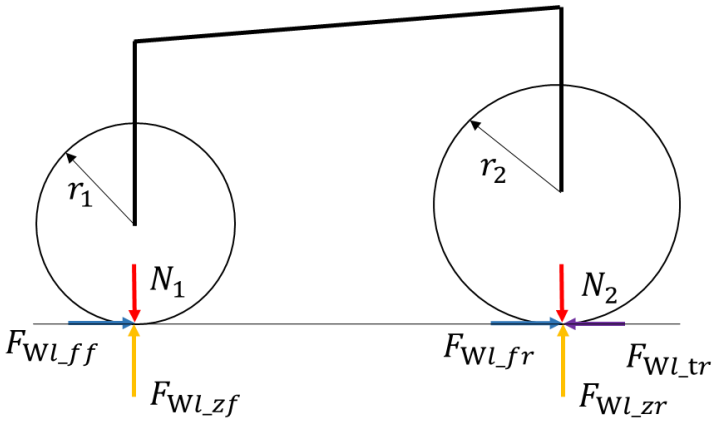

Figure 4. The forces on the EWL when driven by rear wheel

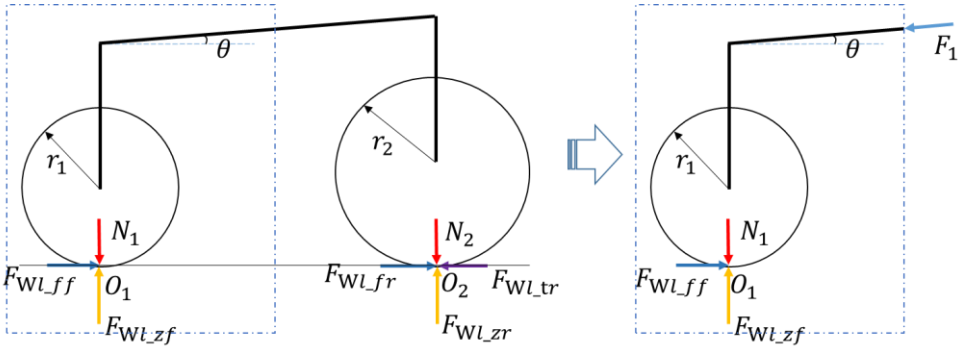

Figure 5. The forces on front-wheel system when rear-wheel drive

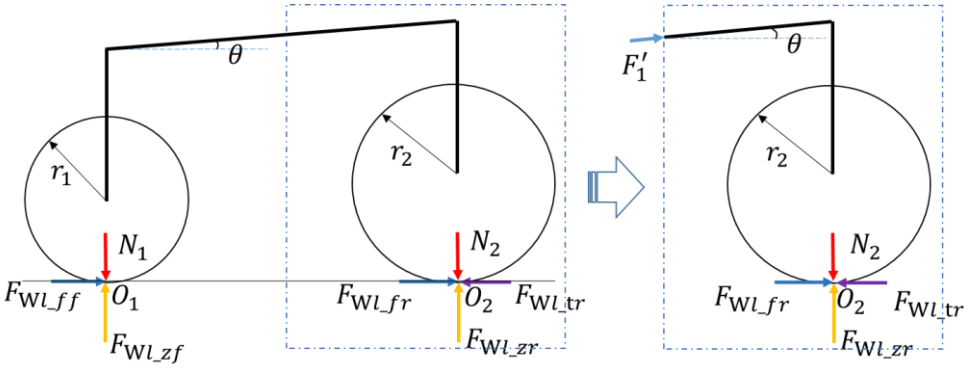

Figure 6. The forces on rear-wheel system when rear-wheel drive

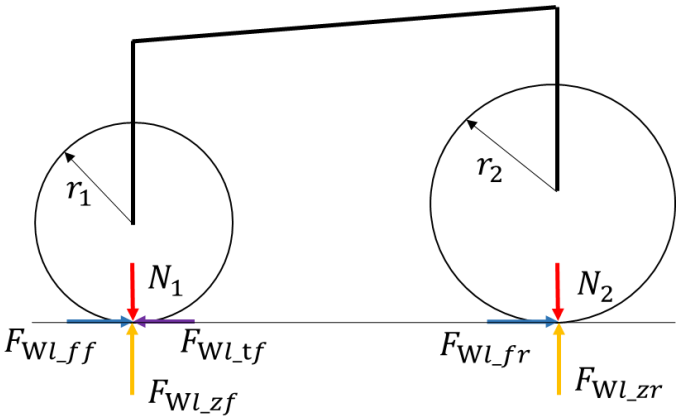

Figure 7. The forces on the EWL when driven by front wheel

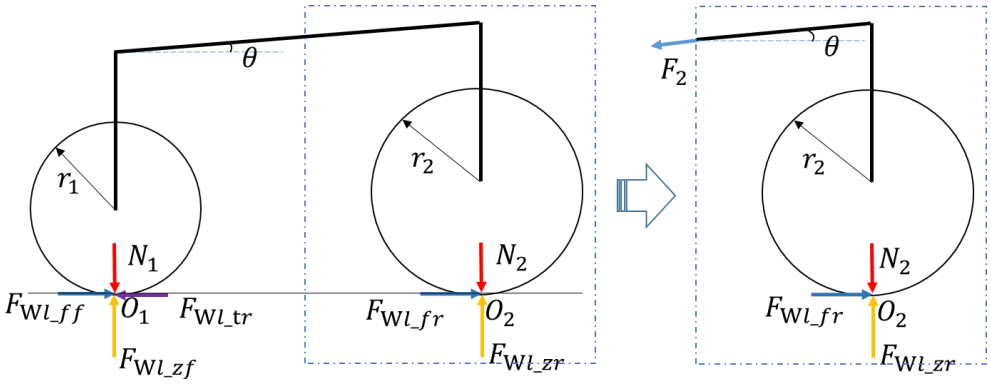

Figure 8. The forces on rear-wheel system when front-wheel drive

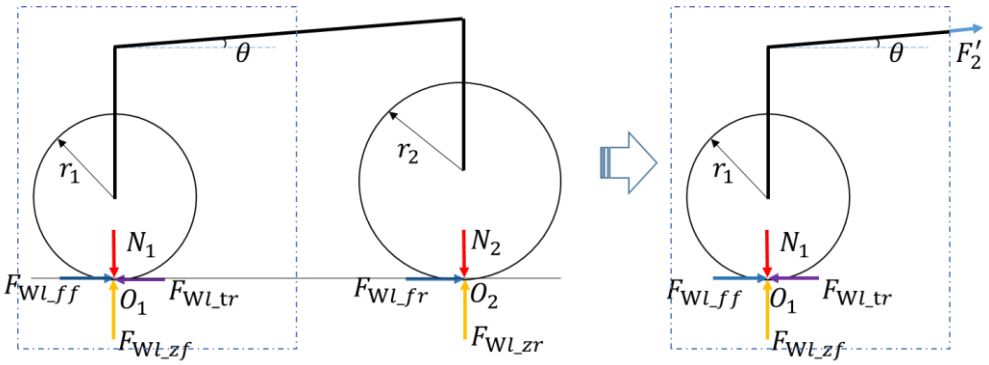

Figure 9. The forces on front-wheel system when front-wheel drive

In the rear-wheel system, the contact point between the tire and the ground is O_2. The forces acting on point O_2 is shown in **Figure 9**. According to Eq. (3) , Eq. (4) and Eq. (5), the force equilibrium of point O_2 can be expressed by Eq. (7). Among them, the reaction force F_{Wl_tr} of the ground to the rear wheel is equal to the driving force F_{t2} generated by the rear-drive torque T_{tq2}.

In Eq. (6) and Eq. (7), θ is the angle between the direction of the interaction force generated by the equivalent connection of the front and rear parts and the horizontal direction, and i_2 is the transmission ratio from the rear drive motor to the drive wheel.

$$\begin{cases} F_{Wl_{ff}} = F_1 \cdot cos\theta \\ F_{Wl_{zf}} = N_1 - F_1 \cdot sin\theta \\ F_{Wl_{ff}} = F_{Wl_{zf}} \cdot f \\ F_1 = F_1' \end{cases} \tag{6}$$

$$\begin{cases} F_{Wl_{tr}} = F_1' \cdot cos\theta + F_{Wl\_fr} \\ F_{Wl\_zr} = N_2 + F_1' \cdot sin\theta \\ F_{Wl\_fr} = F_{Wl\_zr} \cdot f \\ F_{Wl\_xr} = \dfrac{T_{tq2}}{r_2} \cdot i_2 \end{cases} \tag{7}$$

Combining Eq. (6) and Eq. (7), the driving torque T_{tq2} of rear-drive motor can be expressed by Eq. (8).

$$T_{tq2} = \frac{f \cdot (N_1 + N_2) \cdot r_2}{i_2} = \frac{Gfr_2}{i_2} \tag{8}$$

The calculating process of rolling resistance of the front wheel is shown in Eq. (9). And the calculating process of rolling resistance of the rear wheel is shown in Eq. (10). The rolling resistance of front wheel is deduced as in Eq. (11). The rolling resistance of rear wheel is deduced as in Eq. (12). Secondly, the similar formula can be derived to express the driving torque T_{tq1} of the front-drive motor, as shown in Eq. (13). Based on Eq. (13), i_1 is the transmission ratio from the front drive motor to the drive wheel. G is the total gravity of EWL. By sorting out the Eq. (9) to Eq. (13), Eq. (14) and Eq. (15) can be obtained.

From the theoretical analysis, three conclusions can be drawn as follows.

1. The expression of rolling resistance of the front wheel and that of the rear wheel is the same, whether the EWL is driven by the front wheel individually or by the rear wheel individually. Eq. 16 represents the rolling resistance of the

front wheel, and Eq. (17) represents the rolling resistance of the front wheel.

2. Whether the EWL is front-wheel drive or rear-wheel drive, the resistance to be overcome on the drive wheel is the same and is not affected by the radius of the front or rear wheels. This can be expressed in Eq. (18).
3. When the front and rear wheels drive simultaneously, the rolling resistance of the front wheel can be calculated by Eq. (19) the rolling resistance of the rear wheel can be calculated by Eq. (20).

The reaction force from the ground on the front wheel in the horizontal direction can be expressed by Eq. (21). And the reaction force from the ground on the rear wheel in the horizontal direction can be expressed by Eq. (22). The equivalent interaction force between the front-wheel system and the rear-wheel system is F_{σ}, which is expressed by Eq. (23).

3.4. Driving Performance in Shoveling Condition

Based on the forces in **Figure 3** and given in the formulas above, new driving performance is probably to be conducted when the external forces on EWL increase in shoveling condition. The dire ction of resultant force on the tip of the bucket is shifted up and down when the EWL works in shoveling condition, which makes the external force of the bucket constantly change. Therefore, there are two cases to discuss.

First, when the direction of F_{Bct_y} is upward, the front wheel of EWL will be lifted up if F_{Bct_y} is large enough leading the Eq. (24) be in being. In this case, the EWL can move forward with power if it is rear-wheel driven, for the drive force from the ground on rear wheel grows with the increasing positive pressure N_2. However, the front wheel will probably to slip for the center of gravity moves backward along with the increasing force F_{Bct_y} on the bucket, if the EWL is front-wheel driven. The slippage occurs as long as the ground adhesion is lower than the driving force of the front wheel, and this satisfies the Eq. (25).

Parasitic power will be generated when the front wheel slips, which consumes enormous kinetic energy and aggravates tire wear [35]. If F_{Bct_y} is large enough, the front wheels will be propped up to idle running. In this case, if the EWL is driven by the front wheels, there is no driving force. Therefore, the EWL will be difficult to move forward because of lack of power.

$$F_{Wl\_ff} = (N_1 - F_1 \cdot sin\theta) * f = F_1 \cdot cos\theta \tag{9}$$

$$F_{Wl\_fr} = (N_2 + F_1' \cdot sin\theta) \cdot f = \left(\frac{Ga}{l} + F_1' \cdot sin\theta\right) \cdot f = \left(\frac{Ga}{l} + \frac{f \cdot N_1}{f \cdot sin\theta + cos\theta} \cdot sin\theta\right) \cdot f \tag{10}$$

$$F_{Wl\_ff} = \frac{G \cdot f \cdot b}{(f \cdot tan\theta + 1)l} = \frac{G \cdot f \cdot b}{\left(f \cdot \frac{r_1 - r_2}{l} + 1\right)l} = \frac{G \cdot f \cdot b}{f(r_1 - r_2) + l} \tag{11}$$

$$F_{Wl\_fr} = \frac{G \cdot f(f \cdot l \cdot tan\theta + a)}{(f \cdot tan\theta + 1) \cdot l} = \frac{Gf[f(r_1 - r_2) + a]}{f(r_1 - r_2) + l} \tag{12}$$

$$T_{tq1} = \frac{f \cdot (N_1 + N_2) \cdot r_1}{i_1} = \frac{Gfr_1}{i_1} \tag{13}$$

$$F_{Wl\_ff} = \begin{cases} \dfrac{Gf[f(r_1 - r_2) + b]}{f(r_1 - r_2) + l} & (Driven\ by\ Front\ wheels) \\ \dfrac{G \cdot f \cdot b}{f(r_1 - r_2) + l} & (Driven\ by\ Rear\ wheels) \end{cases} \tag{14}$$

$$F_{Wl\_fr} = \begin{cases} \dfrac{G \cdot f \cdot a}{f(r_1 - r_2) + l} & (Driven\ by\ Front\ wheels) \\ \dfrac{Gf[f(r_1 - r_2) + a]}{f(r_1 - r_2) + l} & (Driven\ by\ Rear\ wheels) \end{cases} \tag{15}$$

Second, when the direction of F_{Bct_y} is downward, the rear wheel of EWL will be lifted up if F_{Bct_y} is large enough leading the Eq. (26) be in being.

In this case, the EWL can move forward with power if it is front-wheel driven, for the drive force from the ground on rear wheel grows with the increasing positive pressure N_1. However, the rear wheel will probably to slip for the center of gravity moves forward along with the increasing force F_{Bct_y} on the bucket, if the EWL is rear-wheel driven. The slippage occurs as long as the ground adhesion is lower than the driving force of the rear wheel, and this satisfies the Eq. (27).

$$F_{wl\_ff} = \frac{Gfb}{l} \tag{16}$$

$$F_{wl\_fr} = \frac{Gfa}{l} \tag{17}$$

$$F_{wl\_f} = G \cdot f \tag{18}$$

$$F_{ff} = (N_1 - F_1 sin\theta)f \tag{19}$$

$$F_{fr} = (N_2 + F_2 sin\theta)f \tag{20}$$

$$F_{xf} = (N_1 - F_1 sin\theta)f - F_1 cos\theta \tag{21}$$

$$F_{xr} = (N_2 + F_2 sin\theta)f + F_2 cos\theta \tag{22}$$

$$F_{\sigma} = \frac{F_{xf} - F_{xf} - (N_1 - N_2)f}{2(cos\theta + f \cdot sin\theta)} \tag{23}$$

$$F_{Bct\_y} \cdot (l_{Br} + l) - G \cdot a - F_{Wl\_zf} \cdot l \geq 0 \tag{24}$$

$$N_1 * f < F_{Wl\_tf} \tag{25}$$

$$F_{Bct\_y} \cdot l_{Bf} - G \cdot a - F_{Wl\_zr} l_f \geq 0 \tag{26}$$

$$N_2 * f < F_{Wl\_tr} \tag{27}$$

Figure 10. The state of the front wheel being supported

Figure 11. The state of the rear wheel being supported

Based on the analysis in Figure 10 and Figure 11, a scientific problem is put forward, there will be disadvantages if an EWL is driven by two motors simultaneously without proper control. If an EWL is driven by two motors assembled on the front and rear axles, and the motors are controlled by a MCU, which outputs the currents of changeable frequency and size to the motors according to the signal of the driver stepping on the accelerator or the brake pedal, the precise control of motors is hardly to obtain, resulting in the front motor or rear motor work to produce parasitic power or motor idling. In the selection and matching of motors to EWL, there will also be increased cost due to excessive motors.

4. Experiment and Tests

In order to verify the correctness of the theoretical derivation in formal part, experiments were carried out to obtain the driving torque and vehicle speed of EWL in the working process. Due to the limitation of the experimental conditions, two types of experiments are realized to get different data for calculation and analysis. One is a free shoveling test for obtaining distributed drive EWL parasitic power and the other is a test for acquiring driving forces under different driving modes.

4.1. Selection of Testing Object

The test object is a ZL50GV-EV type of distributed EWL produced by a Chinese company, as shown in Figure 12. Its rated load of shoveling is 5.3 ton, equipped with three motors, distributed as front drive motor, rear drive motor and hydraulic motor, wherein the two drive motors are not mechanically connected to achieve independent drive and simultaneous drive, shown in Figure 13. The specific parameters are shown in Table 3.

Figure 12. The DEWL for test

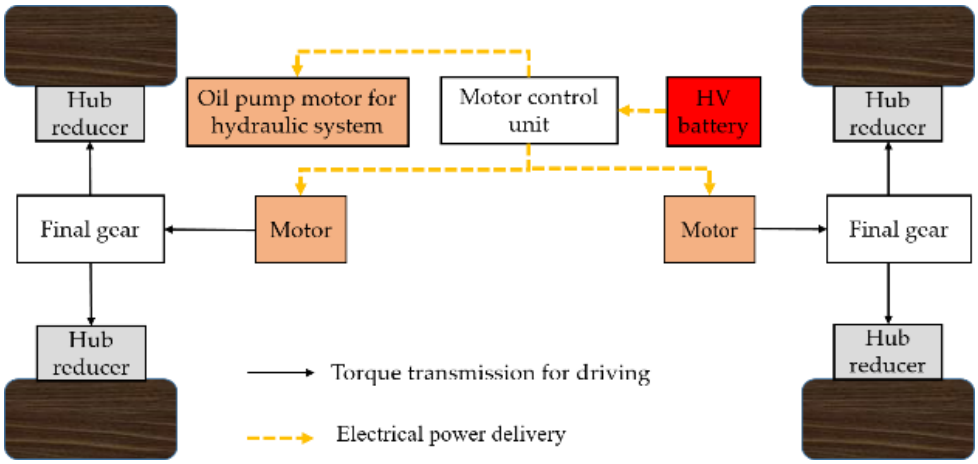

Figure 13. The structure of the testing EWL

Table 3. Parameters of the testing EWL

Parameters	Value	Unit
Rated load	5300	kg
Volume of bucket	3.2	m^3
Rated power of Motor	200	kW
Max torque of Motor	2800	Nm
High efficiency range of Motor	800-3200	rpm
Mass of the vehicle	17000±300	kg
Wheelbase	3300	mm
Axle track	2250	mm
Maximum shoveling force	175±5	kN
Maximum traction force	165±5	kN
Type of tires	23.5-25-16PR	/
Tire diameter	1610	mm
Overall dimensions (L * W* H)	8655*2996*3515	mm
Resultant gear ratio	22.85	/

4.2. Hardware and Software for Test

4.2.1. Hardware for Testing

The hardware of the testing system contains Vehicle Control Unit (VCU), Front Motor Control Unit, Rear Motor Control Unit, Hydraulic Motor Control Unit, Battery Management System, Upper Computer, Data Storage Unit (DTU) and Heat Management Unit. The upper computer collects the information of vehicle status and outputs the control information to the VCU, and controls the motion of the vehicle through the VCU. As a storage device, DTU collects data information via CAN bus. All hardware communicates through the CAN bus with a baud rate of 250 kb/s and the two terminal resistance are both 120 Ohms. The network topology of the hardware system is shown in **Figure 14**.

4.2.2. Software for Testing

In the test, the control programs for driving and shoveling of EWL are compiled by Matlab/Simulink. The drive motors are controlled by VCU. According to the accelerator pedal signal and gear signal, the corresponding frequency and current are output to the motors to drive the WL. The application layer software of the VCU is developed by Matlab/Simulink. There are two types of driving test mode in the programme, including torque control and speed control, with the latter selected as the test programme. It can set three different modes of front motor drive, rear motor drive and dual motor drive, and can also set the target speed of the front and rear motors. The regenerative braking strategy is only accessible in the dual motor drive mode and not in the single motor drive modes, regardless of whether the wheel loader is moving forward or backward. A gentle acceleration rate of 1/50 is set under the control to avoid uncomfortable driving. The wheel speeds can be observed during real vehicle tests. **Figure 15** shows a Simulink graph of the forward mode. In addition, there are electric drive system power-on, power-off control procedures.

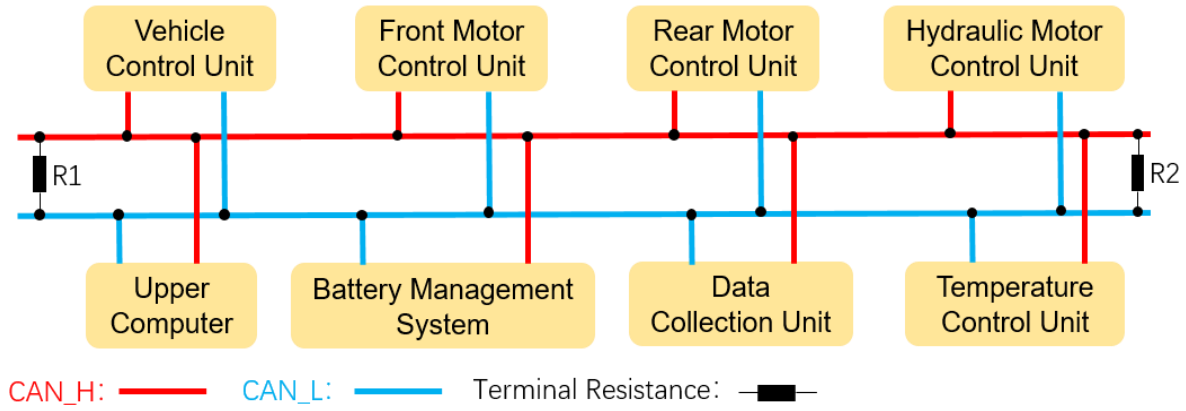

Figure 14. The network topology of the hardware system

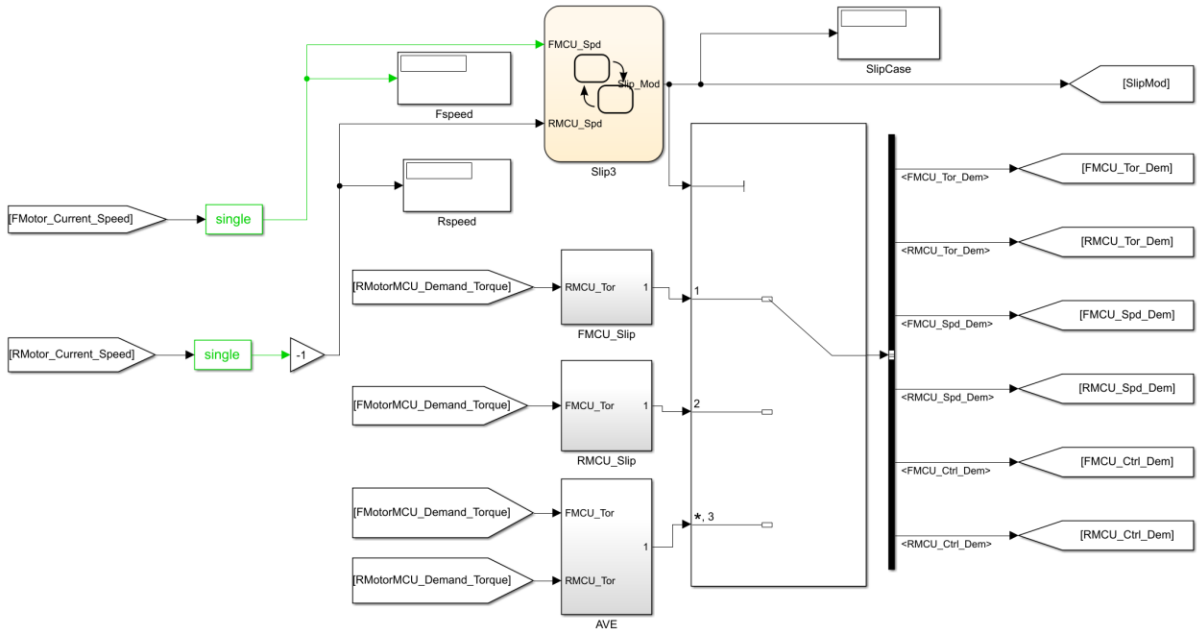

Figure 15. One part of drive mode control program of EWL

4.3. Test Conditions

4.3.1. Test of Free Shoveling

The EWL is set to shovel materials in a driver-operation state, that a skilled driver operates the EWL with dual-axis drive to shovel dry sandstone. In order to ensure the stability of the measurement, the driver only excavates and shovels the materials in front of the material pile, and there is no stage of transporting the material to the truck. The driver should ensure that the loader is in a straight line motion when shoveling for avoiding the influence of steering. The EWL moves on well-paved gravel road with a rolling resistance coefficient of 0.018. This group of experiment aims to obtain the rotation speed and torque of the front and rear motors of the loader, verifying the presence of DEWL parasitic power.

4.3.2. Test of Drive Force

This case is to set the EWL run at three different drive mode, without any weight block or materials in the bucket, of which the tip is 10 cm height from the ground. An ordinary driver drive the EWL run at 600 rpm of the motor speed, which is set by the control system. The first set of experiments is that the EWL is driven by the rear motor alone three times forward and backward. The second set is that the EWL is driven by the rear motor alone three times forward and backward. And the third set is that the EWL is driven by both the front and the rear motor three times forward and backward. Each one-way driving stops when the speed is stable around 600rpm for more than 10 seconds in order to eliminate the influence of acceleration resistance F_j. All the experiment in this case are finished on horizontal hardened cement pavement in straight line.

4.3.3. Data Acquisition

A DTU onboard CAN-bus data recorder with a sampling rate of 100Hz is applied to acquire and record data (**Figure 16**). The data includes the speed and torque of the motors. The unit of speed is rpm, and the unit of torque is N·m.

5. Results Analysis

5.1. Results of Shoveling Condition

The speed and torque curves of the front and rear motors of the DEWL during three times of free shoveling condition are shown in **Figure 17** to **Figure 22**. The speed curves are demonstrated in the same figure and the torque curves are put in the same figure, aiming the convenience for comparison. In the figures, FMCU_Tor represents the torque curve of front motor, RMCU_Tor represents the torque curve of rear motor, FMCU_Sped represents the speed curve of front motor, RMCU_Sped represents the speed curve of rear motor.

It can be seen from the torque curves in **Figure 17** that before the DEWL is going to shovel materials,

the torque of the front and rear motors are almost the same in most cases. However, from 4.8 second to 5.2 second, the bucket has a very short shovel to the ground. As is shown in **Figure 18**, the front speed quickly increases from 10 to 66 rpm while the front torque does not change significantly, and the rear speed keeps on 24 or 25 rpm. The rear torque is higher than the front and both are less than 500 N·m. At about 2.9 second, when the DEWL began to shovel materials, both the front and rear torques increase significantly, and the speeds are almost less than 50 rpm. After 6.8 second, the rear speed is on the rise, while the front speed decreases. Between 6.8 second and 8.8 second, the rear speed is always higher than the front. In the first shoveling, the maximum torque of the front motor is about 1910 N·m, the maximum torque of the rear wheel is about 1780 N·m, and the high torques have a certain holding time.

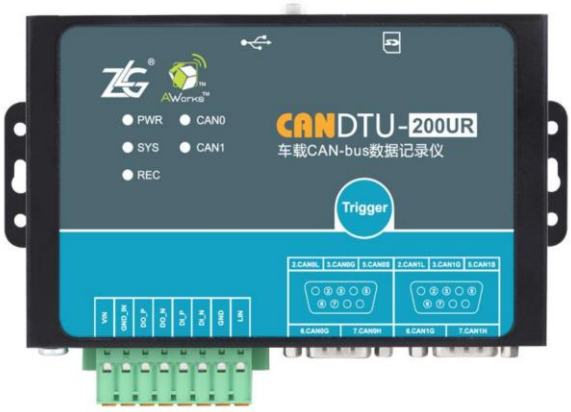

Figure 16. CAN DTU-200UR for Data acquisition

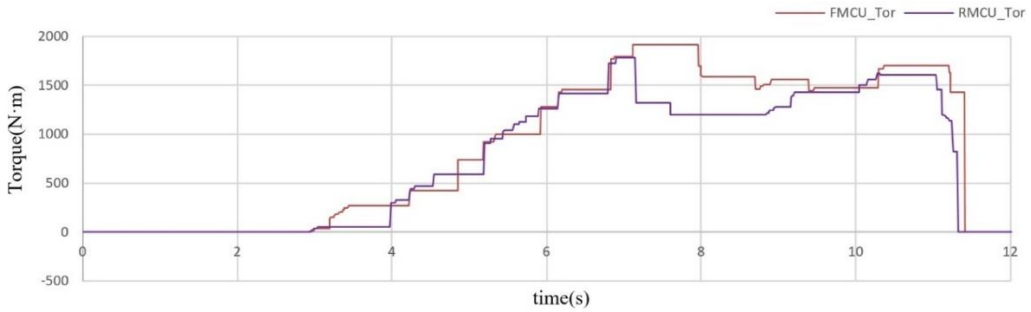

Figure 17. The torque curves of motors in the first free shoveling

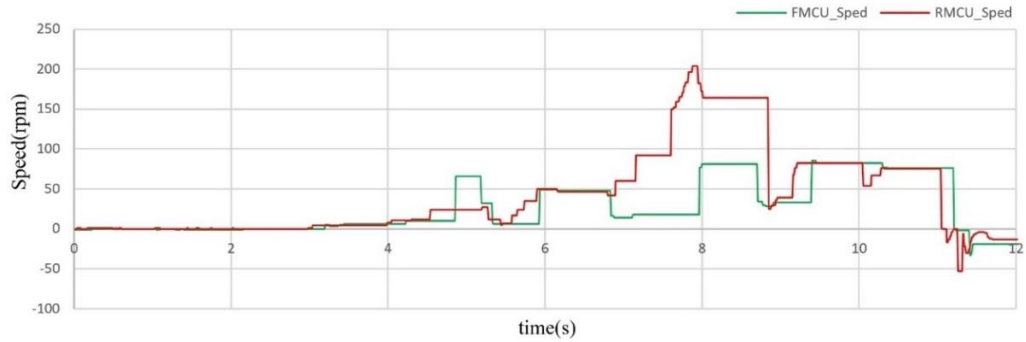

Figure 18. The speed curves of motors in the first free shoveling

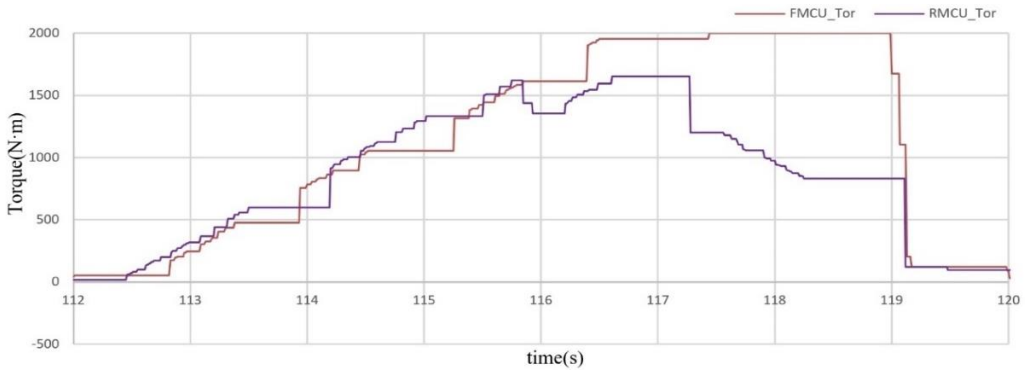

Figure 19. The torque curves of motors in the second free shoveling

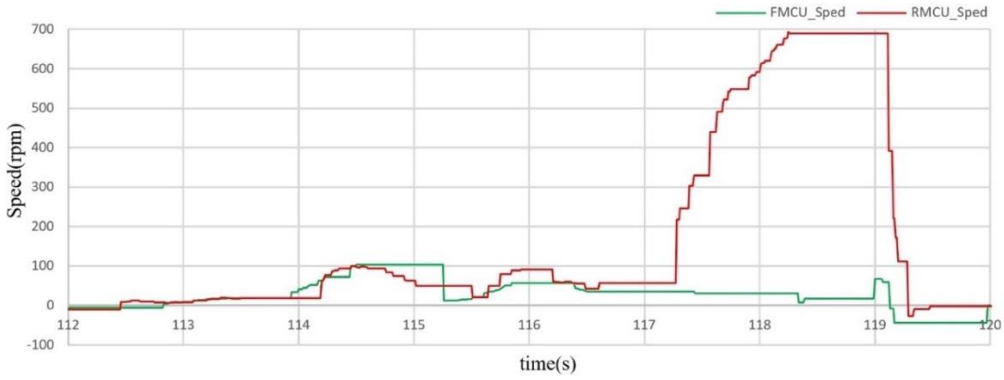

Figure 20. The speed curves of motors in the second free shoveling

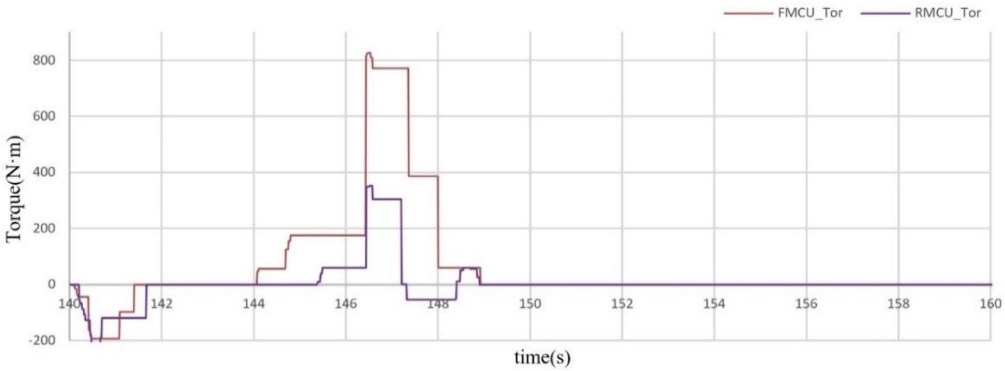

Figure 21. The torque curves of motors in the third free shoveling

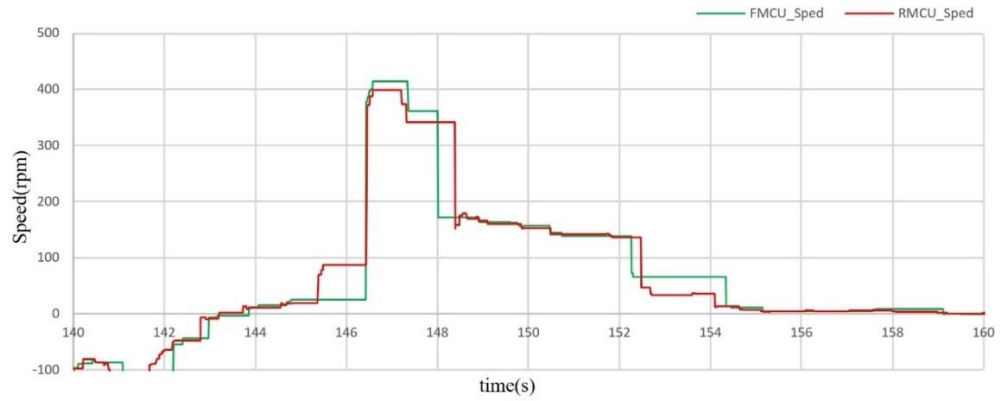

Figure 22. The speed curves of motors in the third free shoveling

During the second shoveling, the maximum front torque appeared between 116.5 second and 119 second, reaching at 2000 N·m, and the maximum rear torque also reaches nearly 1654 N·m, shown in **Figure 19**. Starting from 117.25 seconds, the rear speed increases significantly up to nearly 700 rpm, while the front speed is generally less than 30 rpm, shown in **Figure 20**. From the torque curve, it can be analyzed that the front wheel needs more torque to balance the rolling resistance when the DEWL is inserted into the material pile to shovel the material. This is because the center of gravity of the DEWL moves forward during the shoveling, causing the rise of positive pressure loaded on the front wheel, and the more driving torque should be accordingly provided.

In the third shoveling, the inequality of torques and of speed still exit, but the least obvious among the three shoveling operations.

It can be seen from the speed curve that before digging the material in the pile, the wheel speed increases with the rise of the front and rear wheel drive torque. When the wheel speed decreases

rapidly, it indicates that the bucket has reached the pile. With the increase of torque, the wheel speed is very low, which indicates that the EWL is slow. When the current wheel torque exceeds the rear wheel torque, it is found that the front wheel speed does not change significantly but the rear wheel speed rises sharply, which indicates that the rear wheel has slipped. However, because the rear wheel torque has been output, it indicates that the rear wheel has not left the ground idle, so it can be judged that the rear wheel has generated parasitic power and wasted energy.

5.2. Results of Running Condition

5.2.1. Driven by the Rear Motor Alone

There are three drive modes in running condition. The torque and speed curves of rear drive are presented in **Figure 23**. It can be seen that the actual torque of the rear motor fluctuates greatly when the EWL changes from a stationary state to a stable speed state, because the rolling resistance is unstable during this process. After the current motor speed is stable at 600 rpm, the fluctuation of rear motor torque reduces significantly. The torque of the front motor is zero all across, indicating that it is not involved in the drive.

Three groups of data that are acquired during smooth fluctuation period of torque in forward drive and backward drive are selected to analyze. The selected curves of torque are shown in **Figure 24**.

According to the selected curves, related data can be screened. The average torque $\bar{T}_r$, average $\bar{P}_r$, average torque fluctuation $\Delta\bar{T}_r$, and average power fluctuation $\Delta\bar{P}_r$ can be calculated by Eq.(28) to Eq.(31) and the results are listed in **Table 4**. The calculation for forward motion and reverse motion of the EWL are calculated separately.

$$\bar{T}_r = \frac{\sum_j^k T_i}{k-j+1} \tag{28}$$

$$\bar{P}_r = \frac{\sum_j^k T_i \cdot n_i}{9550 \cdot (k-j+1)} \tag{29}$$

$$\Delta\bar{T}_r = \frac{\left|Av_{\bar{T}_r} - \bar{T}_r\right|}{Av_{\bar{T}_r}} * 100\% \tag{30}$$

$$\Delta\bar{P}_r = \frac{\left|Av_{\bar{P}_r} - \bar{P}_r\right|}{Av_{\bar{P}_r}} * 100\% \tag{31}$$

Based on Eq. (28), T_i is the i th torque of the motor in the collected data. k is the sequence of the initial data of the data segment, and j is the sequence of the final data of the data segment. In Eq. (29), n_i is the i th speed of the motor in the collected data. Furthermore in Eq. (30), $Av_{\bar{T}_r}$ is the average value $\bar{T}_r$ of calculated for each data segment in the table, which is equal to the average value of $\bar{T}_r$ for three forward or three backward stages and in Eq. (31), $Av_{\bar{P}_r}$ is the average value $\bar{P}_r$ of calculated for each data segment in the table, which is equal to the average value of $\bar{P}_r$ for three forward or three backward stages.

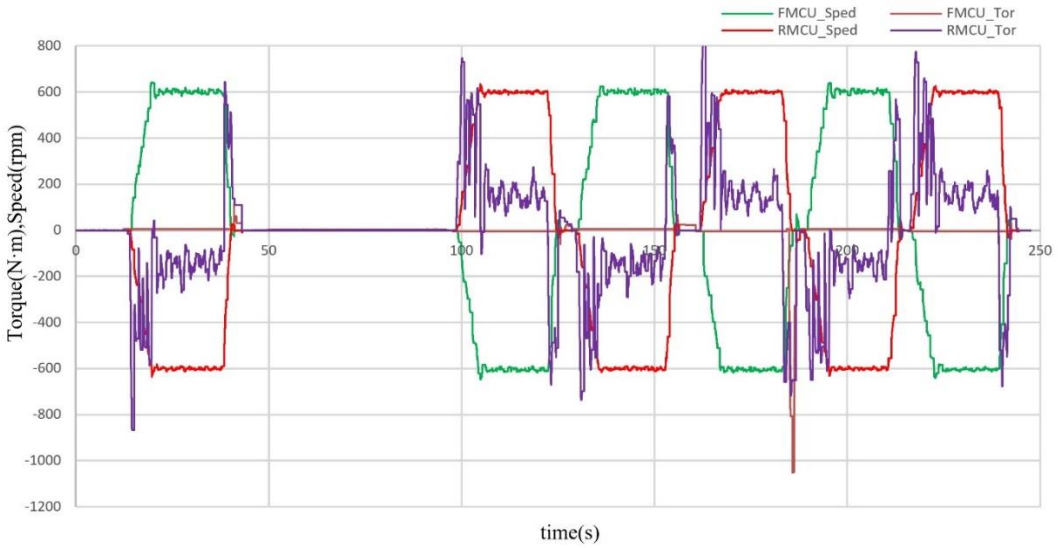

Figure 23. The torque and speed curves of rear driven condition

In the three cases of EWL moving forward, the average torque is 149.95 N·m, and the average torque fluctuations are less than 0.74%. The average power is 9.42 kW, and the power fluctuations are less than 0.72%. In the three cases of EWL moving backward, the average torque is 149.36 N·m, and the average torque fluctuations are less than 1.28%. The average power is 9.37 kW, and the power fluctuations are less than 1.29%.

5.2.2. *Driven by the Front Motor Alone*

Similarly, the data of the smooth fluctuation section of torque in the front drive test are selected, and the torque distribution is shown in **Figure 25**. The average torque $\bar{T}_f$, average power $\bar{P}_f$, average torque fluctuation $\Delta\bar{T}_f$ and average power fluctuation $\Delta\bar{P}_f$ of the front motor in each data section are shown in **Table 5**. The calculation method is consistent with the previous group.

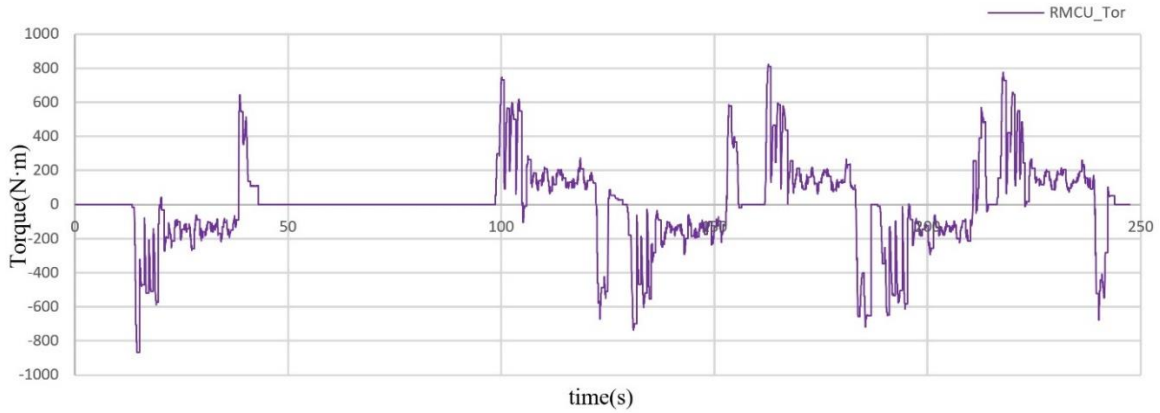

Figure 24. The torque curves of rear driven condition

Table 4. Data calculated in rear drive mode

Data segment	$\overline{T_r}$ (N·m)	$\overline{P_r}$ (kWh)	$\Delta\overline{T_r}$	$\Delta\overline{P_r}$	Vehicle state
2175-3629	149.08	9.36	0.58%	0.57%	Forward
13829-15175	149.71	9.40	0.16%	0.15%	Forward
20270-21004	151.07	9.49	0.74%	0.72%	Forward
10752-12086	147.98	9.28	0.93%	0.96%	Backward
16933-18187	151.28	9.49	1.28%	1.29%	Backward
22564-23875	148.83	9.34	0.36%	0.32%	Backward

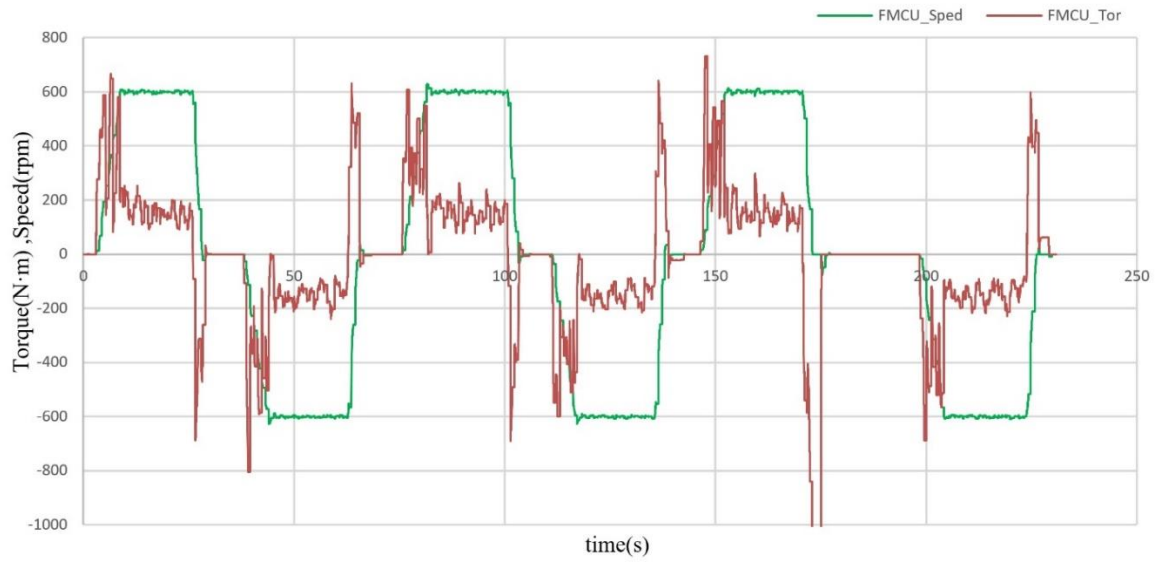

Figure 25. The torque and speed curves of front driven condition

Table 5. Data calculated in front drive mode

Data segment	$\overline{T_f}$ (N·m)	$\overline{P_f}$ (kWh)	$\Delta\overline{T}_f$	$\Delta\overline{P}_f$	Vehicle state
1624-2581	149.65	9.37	0.34%	0.14%	Forward
8635-9976	148.87	9.35	0.19%	0.15%	Forward
15605-16985	148.91	9.36	0.16%	0.02%	Forward
4584-6163	151.05	9.49	0.17%	0.20%	Backward
11850-13547	151.35	9.51	0.37%	0.35%	Backward
20443-22173	150.00	9.42	0.53%	0.55%	Backward

In the three cases of EWL moving forward, the average torque is 149.14 N·m, and the average torque fluctuations are less than 0.34%. The average power is 9.36 kW, and the power fluctuations are less than 0.15%. In the three cases of EWL moving backward, the average torque is 150.80 N·m, and the average torque fluctuations are less than 0.53%. The average power is 9.48 kW, and the power fluctuations are less than 0.55%.

By comparing the data at the front and rear drive cases, it can be found that the motor output torque is between 149 N·m and 151N·m, no matter the EWL is front drive or rear drive, no matter whether the EWL is in the forward or reverse process. The torque fluctuation and power fluctuation are stable in a very small range from 0.16 % to 1.28 %, and the consumed power fluctuation is stable in a small range from 0.02 % to 1.29 %. It shows that under the configuration of single front drive and single rear drive, the effect is the same in terms of energy consumption and driving force under the premise the same overall transmission ratio.

5.2.3. *Driven by Dual Motor Simultaneously*

The EWL works in the speed control mode in dual-drive mode. The target speed of the two motors is set to be 600 rpm, the front and rear motors both generate torques which are uncontrolled. The curves of torque and speed are shown in **Figure 26**.

It is set before experiment realizing that in the process of driving forward, when the motor generates torque to drive, the torque value is positive, when the motor is dragged back, the torque value is negative. But in the process of reversing, the torque value is negative when the motor generates out torque, while the torque value is positive when the motor is dragged back.

The average torque of front motor $\overline{T}_f$, the average torque of rear motor $\overline{T}_r$ are calculated as the former cases and the results are shown in **Table 6**. $\overline{T_\Delta}$ is the algebraic sum of $\overline{T}_f$ and $\overline{T}_r$ in each data segment, which represents the overall drive torque on the EWL. $\overline{P}_s$ is the average power of the sum of that generated or regenerated by the motors in the same data segment. The representation of $\overline{P}_s$ can be expressed by Eq. (32).

The average torques of $\overline{T_\Delta}$ are 175 N·m in running forward and 179.31 N·m in running backward, which are much larger than in that of alone driven by the rear motor or the front motor. In addition, the fluctuation of $\overline{T_\Delta}$ reaches 3.42% and 9.52% in running forward and running backward cases respectively, the fluctuation of $\overline{P}_s$ reaches 2.49% and 5.11% in running forward and running backward case respectively, which are also much greater than that of alone driven by single motor. At last, the average powers consuming in the process is 11 kW in running forward cases and 11.49 kW in running backward cases, indicating that the dual-motor driven without proper control has less energy efficiency than that of single motor driven.

$$\overline{P}_s = \frac{\sum_j^k (T_{f_i} \cdot n_{f_i} + T_{r_i} \cdot n_{r_i})}{9550 \cdot (k - j + 1)} \tag{32}$$

6. Discussion

The driving characteristics of DEWL in shoveling condition obtained by theoretical derivation and experimental verification in this study have the following application prospects for the field of DEWLs:

1. For the mounting position of drive motor, it can be determined based on the design of the maximum driving force, transmission ratio, body design space layout and other factors [36], [37]. For small or light EWLs, single motor should be applied if the manufacture cost is taken into consideration.
2. For dual-motor drive EWLs, the occurrence of front wheel tilt or rear wheel tilt, and motor idling or motor overload, should be avoid, which can be achieved in the procedure of design and control program development.

3. Double-motor drive can greatly improve the driving torque and maximum digging force of EWL, but the control of the speed, torque of the motors and the movement motion of EWL, should be well developed to obtain the more convenient and intelligent operation for divers.
4. In order to save more energy, the selection and configuration of motors should be determined on the basis of mechanical properties and energy efficiency of the motors [38], make the EWL can often run in an economic speed range. For EWLs driven by double motors in front and rear axle, the transmission ratios of the front and rear axles can also be changed according to the parameters of the motor to make the motor adaptive to the working conditions of EWLs.
5. Design and research of assisted driving. Unskilled drivers can also achieve good driving performance when operating loaders, reducing the generation of parasitic power, the wear of tires and motor overload conditions.

To improve the drive performance and to decrease the energy consumption based on the characteristics of DEWL in shoveling condition, the challenges for DEWL research in the near future are as follows:

1. How to perceive the slips happen on tires to determine whether parasitic power is generated. In some cases, the tire slip can effectively protect the motor overload. It will probably be a misjudgment in the controlling process between the prevention of parasitic power and the protection of overload of motors. More parameters are expected to play important roles in the coordinate control system.
2. Hydraulic system is not discussed separately in this paper, the hydraulic system also consumes huge energy, especially in the digging process, energy consumption of hydraulic system and walking system should be considered as an interrelated and organic combination of the overall system.

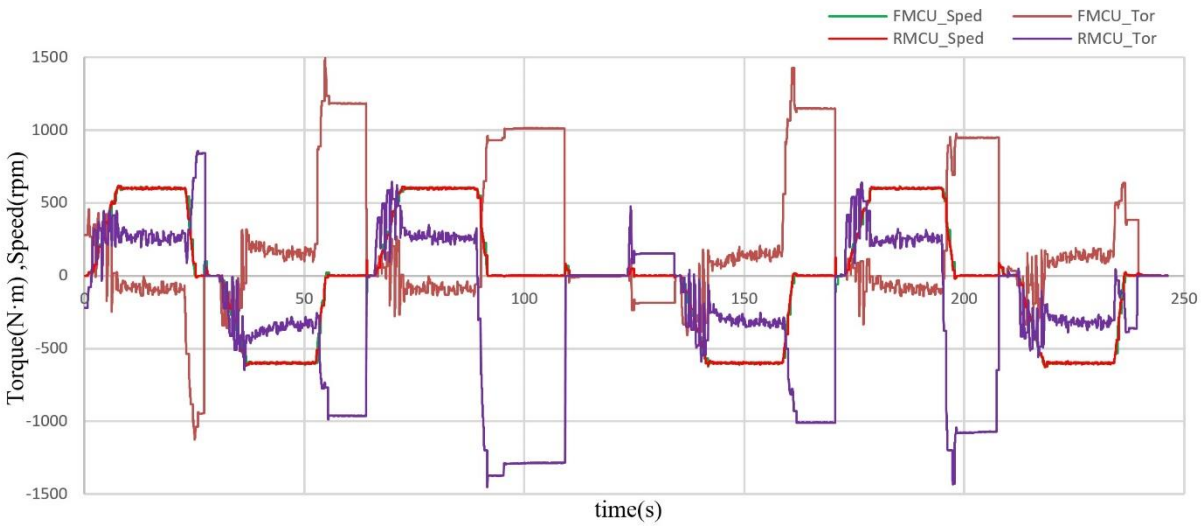

Figure 26. The torque and speed curves of all driven condition

Table 6. Data calculated in dual-motor drive mode

Data segment	$\overline{T_f}$ (N·m)	$\overline{T_r}$ (N·m)	$\overline{T_\Delta}$ (N·m)	$\overline{P_s}$ (kWh)	$\Delta\overline{T_\Delta}$	$\Delta\overline{P_s}$	Vehicle state
858-2208	-85.27	264.85	179.58	11.27	2.15%	2.49%	Forward
7385-8775	-88.51	262.55	174.04	10.96	1.27%	0.40%	Forward
18000-19400	-78.92	250.39	171.47	10.77	3.42%	2.09%	Forward
3650-5350	193.02	-360.76	-167.74	10.92	9.52%	4.92%	Backward
14297-15767	125.54	-308.62	-183.08	11.46	6.31%	0.19%	Backward
22031-23315	131.72	-318.83	-187.10	12.07	3.21%	5.11%	Backward

7. Conclusion

In this study, the DEWL with a front drive motor and a rear drive motor is taken as the research object. By developing dynamic models for DEWL of running and shoveling conditions, the drive forces and the rolling resistances act on the EWL are conducted and analyzed. The paper presents an in-depth study of the drive mechanics characteristics of a DEWL under shoveling conditions from both theoretical analysis and experimental calculations. The following conclusions are drawn:

1. The conditions under which parasitic power is generated during the shoveling process of an EWL, are indicated via mathematical formulas.
2. The rolling resistances on the front and rear wheels of a two-wheel drive EWL with front drive alone or rear drive alone is expressed in an equation, for the first time in this field. And it is proved that the total rolling resistance to the EWL is the same, which is independent of either the radius of the wheels or driven by which axle.
3. It is confirmed through experiments that the torques of motors measured are basically the same with very small fluctuation in either front drive mode or rear drive mode. Meanwhile, the test results show that if there is no appropriate control on the front and rear motors, the effect of energy saving cannot achieve when a DEWL is dual-motor driven.

At present, the energy-saving research on EWL are mainly about the efficiency of batteries [39], the energy recovery [22], the hybrid technology [28] and others [11], [40]. The research ignored the influence of the mechanical characteristics of EWL in its shoveling condition and running condition. In the future, our research will go deeper in the following directions.

1. The elimination of parasitic power of electric loaders, mainly to reduce energy loss and tire wear, and more importantly, to prevent the overload of motors.
2. Electric loader assistant driving, including front and rear drive motors, hydraulic motors and hydraulic system coordination control, in order to improve its operational performance and electricity utilization efficiency.

Acknowledgements

The financial support of this research by The Sudian Yingcai Engineering Project from Jiangsu Vocational College of Electronics and Information, and Huai'an City Science and Technology project (Grant No. HABL202127), Research Youth Fund Program Project of Jiangsu Vocational College of Electronics and Information (Grant No. JSEIYQ2020004) are gratefully acknowledged.

Author's Declaration

Authors' contributions and responsibilities

Fei Xiaotao and Han Shenrui were responsible for conceptualization, data collection and analysis. Wong Shaw Voon and Fei Xiaotao were responsible for methodology, writing review and editing. Fei Xiaotao wrote the first draft of the article. Han Yunwu was responsible for visualization. Wong Shaw Voon was responsible for supervision. Fei Xiaotao was responsible for funding acquisition. Muhammad Amin Bin Azman is responsible for the English edition.

Funding

This work was supported by the < Sudian Yingcai Engineering Project > and < Huai'an City Science and Technology Project > under Grant [number HABL202127] and < Research Youth Fund Program Project of Jiangsu Vocational College of Electronics and Information> under Grant [number JSEIYQ2020004]

Availability of data and materials

All data are available from the authors.

Competing interests

The authors declare no competing interest.

Additional information

The expression of notations in the text: DEWL –Distributed Electric Wheel Loader; EWL –Electric Wheel Loader; PMSM –Permanent Magnet Synchronous Motor; SMR –Switched Reluctance Motor; WL –Wheel Loader;

References

[1] S. Dadhich, U. Bodin, and U. Andersson, "Key challenges in automation of earth-moving machines," *Automation in Construction*, vol. 68, pp. 212–222, 2016, doi: 10.1016/j.autcon.2016.05.009.

[2] S.-H. Lee, C.-S. Song, and C.-K. Chung, "The Characteristic Analysis of the Load-sensitive Hydraulic Control System for Closed Center Type of a Wheel Loader," *Transactions of the Korean Society of Mechanical Engineers A*, vol. 31, no. 9, pp. 934–942, 2007, doi: 10.3795/KSME-A.2007.31.9.934.

[3] W. Zongcai, F. Wude, W. Yun, and L. Zhengguo, "Study on hydraulic system energy saving features for wheel loader typical working condition," *Hydraulic Pneumatic & Seals*, vol. 37, no. 12, pp. 40–42, 2017.

[4] X. Yan, J. Yang, and L. Quan, "Co-simulation and experiment of wheel loader during operation process," *Transactions of the Chinese Society of Agricultural Engineering*, vol. 31, no. 16, pp. 102–109, 2015, doi: 10.11975/j.issn.1002-6819.2015.16.015.

[5] M. Bhola, A. Kumar, and N. Kumar, "Energy-efficient control of hydrostatic transmission of a front-end loader machine using machine learning algorithm and its sensitivity analysis," *Proceedings of the Institution of Mechanical Engineers, Part D: Journal of Automobile Engineering*, p. 09544070221133154, 2022, doi: 10.1177/09544070221133154.

[6] L. Wan, H. Dai, Q. Zeng, Z. Sun, and M. Tian, "Characteristic analysis and co-validation of hydro-mechanical continuously variable transmission based on the wheel loader," *Applied Sciences*, vol. 10, no. 17, p. 5900, 2020, doi: 10.3390/app10175900.

[7] M. Guangliang, W. Liang, and L. Yingying, "Wheel loader engine multi-power mode energy-saving research," *Construction Machinery and Equipment*, vol. 40, no. 03, pp. 20-24+90, 2009.

[8] L. Yanhui, L. Chang, and Y. Guoxiu, "Simulation and experimental study on engine power saving of loader," *Construction Machinery*, vol. 01, pp. 51-53+58, 2017, doi: 10.14189/j.cnki.cm1981.2017.01.004.

[9] W. Haifei, Y. Shuxin, K. Yan, L. Xinwei, Z. Zhonghua, and M. Yangpan, "Simulative research on hydraulic mechanical composite transmission energy-saving system for ZL50 loader," *Xi'an University of Arch & Tech (natural science edition)*, vol. 47, no. 01, pp. 141–146, 2015, doi: 10.15986/j.1006-7930.2015.01.026.

[10] L. Luo, P.-Y. Wang, W. Sun, M.-L. Ba, Z.-H. You, and X. He, "Research on the energy-saving mechanism for the hybrid mechanical loader with parallel power system," in *Design, Manufacturing and Mechatronics: Proceedings of the International Conference on Design, Manufacturing and Mechatronics (ICDMM2016)*, 2017, pp. 282–289, doi: 10.1142/9789813208322_0033.

[11] Z. Lin, F. Wang, and B. Xu, "Improving wheel loader energy efficiency with a series electric hybrid powertrain," in *Fluid Power Systems Technology*, 2022, vol. 86335, p. V001T01A019, doi: 10.1115/FPMC2022-8909.

[12] G. Wu, X. Zhang, and Z. Dong, "Powertrain architectures of electrified vehicles: Review, classification and comparison," *Journal of the Franklin Institute*, vol. 352, no. 2, pp. 425–448, 2015, doi: 10.1016/j.jfranklin.2014.04.018.

[13] X. Jin, L. Shi, and Y. Bian, "Design and research on wheel-driven systems of electric loaders," *Chinese Journal of Construction Machinery*, vol. 8, no. 01, pp. 62-65+71, 2010, doi: 10.15999/j.cnki.311926.2010.01.017.

[14] B. Yang, M. Huang, L. H, and J. Zhang, "Comparative Test Research on Performance of Electric Loader and Traditional Loader," *Construction Machinery Technology & Management*, vol. 33, no. 3, pp. 94–98, 2020.

[15] X. Li, C. Duan, K. Bai, and Z. Yao, "Operating performance of pure electric loaders with different types of motors based on simulation analysis," *Energies*, vol. 14, no. 3, p. 617, 2021, doi: 10.3390/en14030617.

[16] B. Cao, X. Liu, W. Chen, K. Yang, and D. Liu, "Intelligent energy-saving operation of wheel loader based on identifiable materials," *Journal of Mechanical Science and Technology*, vol. 34, pp. 1081–1090, 2020, doi: 10.1007/s12206-020-0209-1.

[17] Z. Yang, J. Wang, G. Gao, and X. Shi, "Research on Optimized Torque-Distribution Control Method for Front/Rear Axle Electric Wheel Loader," *Mathematical Problems in Engineering*, vol. 2017, p. 7076583, 2017, doi: 10.1155/2017/7076583.

[18] G. Gao, J. Wang, T. Ma, Y. Han, X. Yang, and X. Li, "Optimisation strategy of torque distribution for the distributed drive electric wheel loader based on the estimated shovelling load," *Vehicle System Dynamics*, vol. 60, no. 6, pp. 2036–2054, Jun. 2022, doi: 10.1080/00423114.2021.1890153.

[19] P. T. Petrović, Ž. P. Petrović, D. M. Obradović, and M. P. Petrović, "Dynamics of

the tractor (4x2), and the occurrence of parasitic power circulation in the drive (4x4)," *Tehnika*, vol. 70, no. 2, pp. 281–287, 2015, doi: 10.5937/tehnika1502281P.

[20] V. V Vantsevich, "Power losses and energy efficiency of multi-wheel drive vehicles: A method for evaluation," *Journal of Terramechanics*, vol. 45, no. 3, pp. 89–101, 2008, doi: 10.1016/j.jterra.2008.08.001.

[21] Y. Zhiyu, L. Shuang, W. Yunlong, and Y. Han, "Generation Mechanism Analysis and Calculation Method of Loader Parasitic Power Based on Tire Radius Difference," SAE Technical Paper, 2022. doi: 10.4271/2022-01-5102.

[22] H. Mu, Y. Luo, Y. Luo, and L. Chen, "Numerical analysis of energy recovery of hybrid loader actuators based on parameters optimization," in *Actuators*, 2022, vol. 11, no. 9, p. 260, doi: 10.3390/act11090260.

[23] J. Liu, Z.-J. Niu, H. Zhu, and C.-S. Zhao, "Design and experiment of a large-aperture hollow traveling wave ultrasonic motor with low speed and high torque," *Applied Sciences*, vol. 9, no. 19, p. 3979, 2019, doi: 10.3390/app9193979.

[24] K. Pettersson and P. Krus, "Design optimization of complex hydromechanical transmissions," *Journal of Mechanical Design*, vol. 135, no. 9, p. 91005, 2013, doi: 10.1115/1.4024732.

[25] J. Yao, Z. Li, and C. Peng, "Shoveling behavior and resistance of loader bucket," *Construction Machinery and Equipment*, no. 03, pp. 9-14+4-48, 1993.

[26] J. Xiaolin, S. Laide, and B. Yongming, "Design and research on wheel-driven systems of electric loaders," *Chinese Journal of Construction Machinery*, vol. 8, no. 01, pp. 62-65+71, 2010, doi: 10.15999/j.cnki.311926.2010.01.017.

[27] K. Oh, H. Kim, K. Ko, P. Kim, and K. Yi, "Integrated wheel loader simulation model for improving performance and energy flow," *Automation in Construction*, vol. 58, pp. 129–143, 2015, doi: 10.1016/j.autcon.2015.07.021.

[28] I. Shafikhani, "Energy management of hybrid electric vehicles with battery aging considerations: Wheel loader case study," *Control Engineering Practice*, vol. 110, p. 104759, 2021, doi: 10.1016/j.conengprac.2021.104759.

[29] T. Lin, Y. Lin, H. Ren, H. Chen, Q. Chen, and Z. Li, "Development and key technologies of pure electric construction machinery," *Renewable and Sustainable Energy Reviews*, vol. 132, p. 110080, 2020, doi: 10.1016/j.rser.2020.110080.

[30] M. Mitschke and H. Wallentowitz, *Dynamik der kraftfahrzeuge*, vol. 4. Springer, 1972.

[31] D. E. Hall and J. C. Moreland, "Fundamentals of rolling resistance," *Rubber chemistry and technology*, vol. 74, no. 3, pp. 525–539, 2001, doi: 10.5254/1.3547650.

[32] Y. Yu, L. Shen, and M. Li, "Optimum design of working device of wheel loader," in *2010 International Conference on Mechanic Automation and Control Engineering*, 2010, pp. 461–465, doi: 10.1109/MACE.2010.5536399.

[33] M. Guiggiani, "The science of vehicle dynamics," *Pisa, Italy: Springer Netherlands*, vol. 15, 2014.

[34] A. L. Schwab, J. P. Meijaard, and J. D. G. Kooijman, "Lateral dynamics of a bicycle with a passive rider model: stability and controllability," *Vehicle system dynamics*, vol. 50, no. 8, pp. 1209–1224, 2012, doi: 10.1080/00423114.2011.610898.

[35] X. Fei, Y. Han, and S. V. Wong, "An Overview of and Prospects for Research on Energy Savings in Wheel Loaders," *Automotive Experiences*, vol. 6, no. 1, pp. 133–148, 2023, doi: 10.31603/ae.8759.

[36] S. Murata, "Innovation by in-wheel-motor drive unit," *Vehicle System Dynamics*, vol. 50, no. 6, pp. 807–830, 2012, doi: 10.1080/00423114.2012.666354.

[37] M. N. Kumar, V. Jagota, and M. Shabaz, "Retrospection of the optimization model for designing the power train of a formula student race car," *Scientific Programming*, vol. 2021, pp. 1–9, 2021.

[38] E. A. Abdelaziz, R. Saidur, and S. Mekhilef, "A review on energy saving strategies in industrial sector," *Renewable and sustainable energy reviews*, vol. 15, no. 1, pp. 150–168, 2011, doi: 10.1016/j.rser.2010.09.003.

[39] Z. Wu, F. Wang, B. Xu, and W. Fiebig, "An Electric-Hydraulic Hybrid Wheel Loader

With Mode-Driven Control Strategy," in *Fluid Power Systems Technology*, 2022, vol. 86335, p. V001T01A047, doi: 10.1115/FPMC2022-90715.

[40] H. Zhang, F. Wang, B. Xu, and W. Fiebig, "Extending battery lifetime for electric wheel loaders with electric-hydraulic hybrid powertrain," *Energy*, vol. 261, p. 125190, 2022, doi: 10.1016/j.energy.2022.125190.